Influence of pH on Liquid−Liquid Phase Transitions of mixed SOA proxy–inorganic Aerosol Droplets

Yueling Chen[1]& Xiangyu Pei[1], Huichao Liu[1], Yikan Meng[1], Zhengning Xu[1], Fei Zhang[1], Chun Xiong[1], Thomas C. Preston[3], Zhibin Wang[1,2,4*]

[1]College of Environmental and Resource Sciences, Zhejiang Provincial Key Laboratory of Organic Pollution Process and Control, Zhejiang University, Hangzhou 310058, China
[2]ZJU-Hangzhou Global Scientific and Technological Innovation Center, Zhejiang University, Hangzhou 311215, China
[3]Department of Atmospheric and Oceanic Sciences and Department of Chemistry, McGill University, 805 Sherbrooke Street West, Montreal, Quebec H3A 0B9, Canada
[4]Key Laboratory of Environment Remediation and Ecological Health, Ministry of Education, Zhejiang University, Hangzhou 310058, China

Correspondence to: Zhibin Wang (wangzhibin@zju.edu.cn)

Yueling Chen and Xiangyu Pei contribute equally to this work.

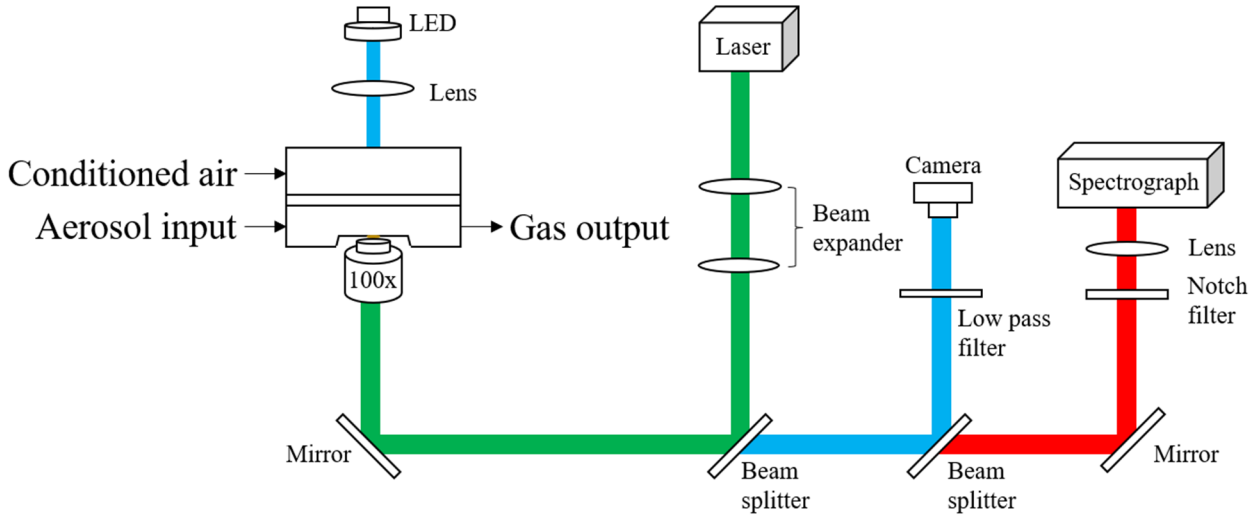

Figure S1. Schematic of aerosol optical tweezer setup used in this study. Medical nebulizer nebulized dissolved solution to generate aerosol droplets. Conditioned airflow is mixed by a dry airflow and a humid airflow that humidified by a water bubbler. A temperature and humidity sensor measured the temperature and RH of the conditioned airflow after it enters the chamber.

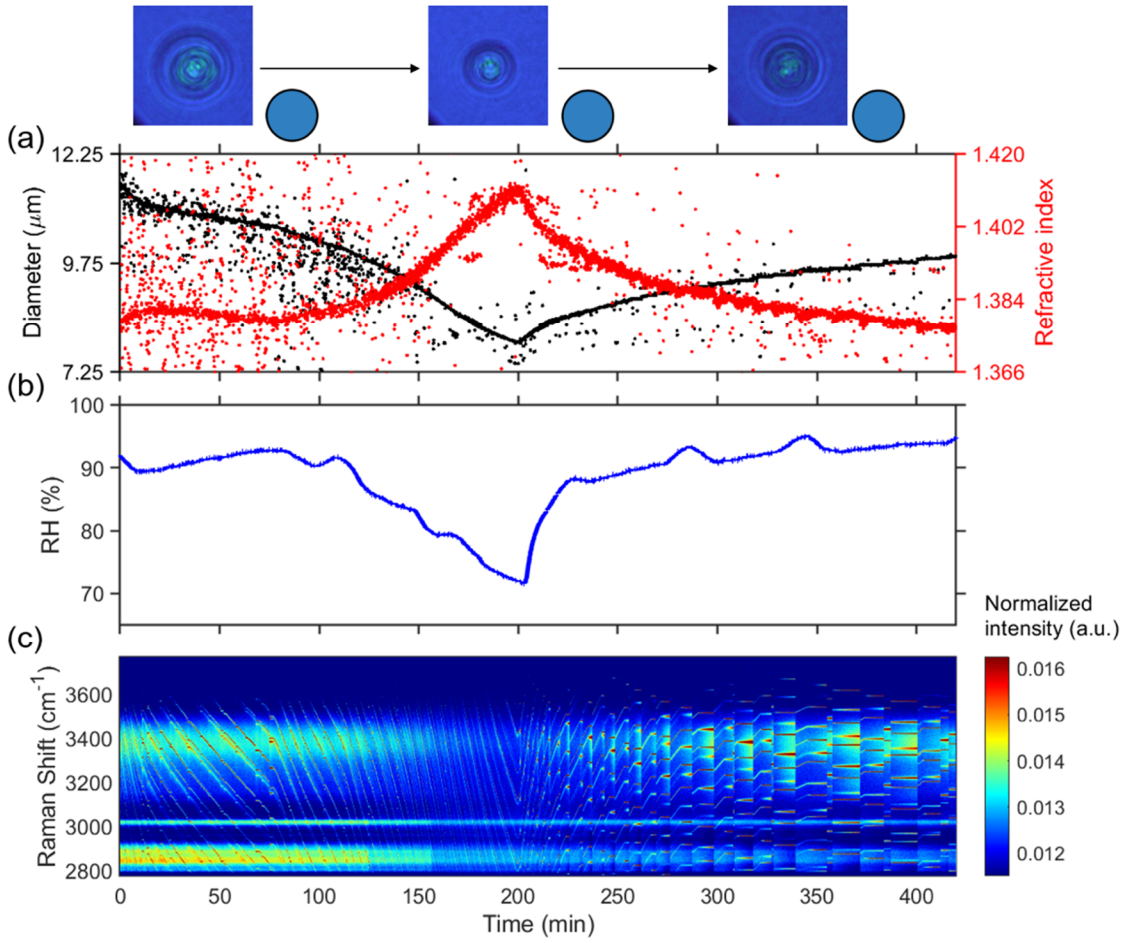

Figure S2. Result of GL/AS system. (a) Timescale of changes in droplet size and refractive index, determined from fitting the Raman shift positions of the WGMs. (b) RH variation after the trapping chamber during the humidity changing process with time. (c) Time-resolved Raman spectra.

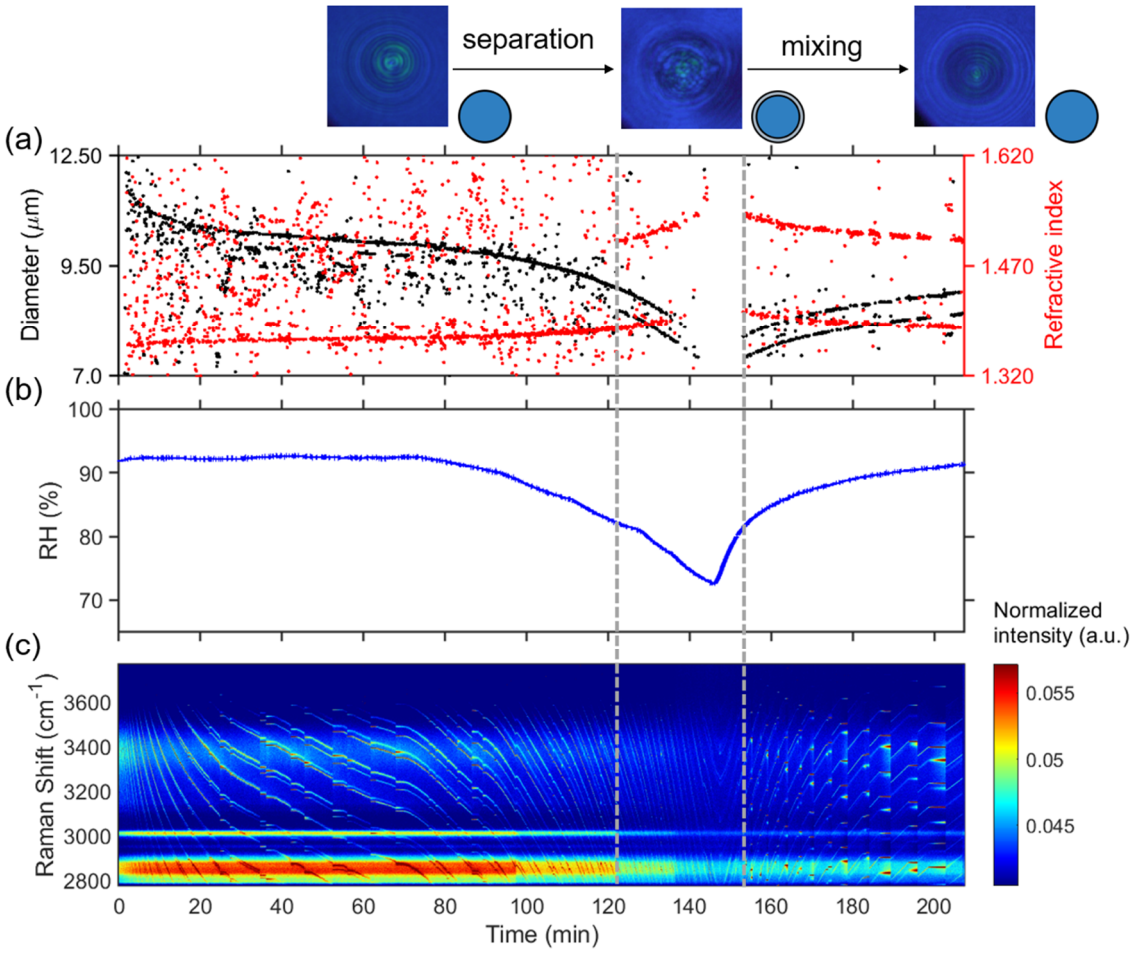

Figure S3. Liquid-liquid phase separation of aqueous of HEXT-IV. (a) Timescale of changes in droplet size and refractive index, determined from fitting the Raman shift positions of the WGMs. (b) RH variation after the trapping chamber during the humidity changing process with time. (c) Time-resolved Raman spectra. The cessation of the random motion of inclusions within the droplet and the resultant formation of a core-shell structure are indicated by the grey dashed line on the left. The grey dashed line on the right serves as an indication of the point at which the droplet morphology transitions from a state of phase separation to a homogeneous phase morphology. This transformation is characterized by the occurrence of phase mixing.

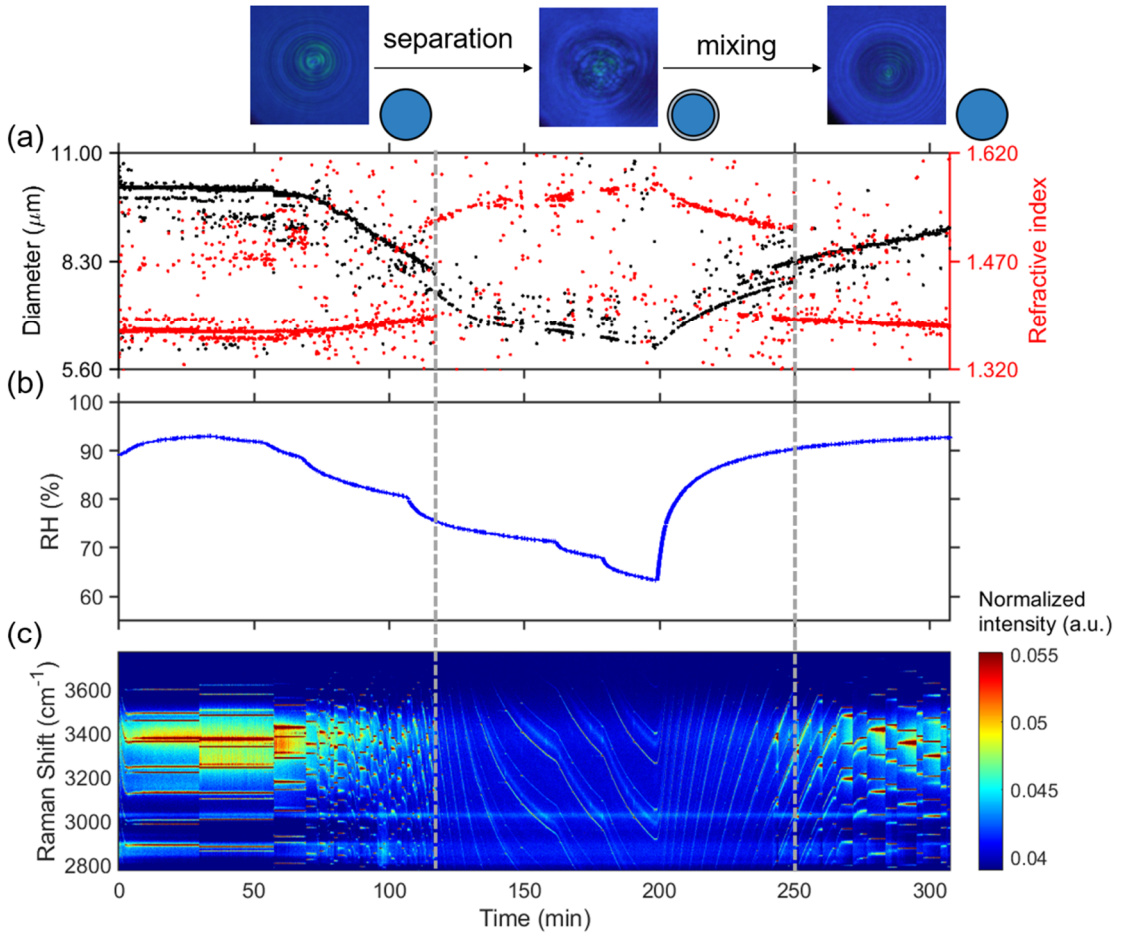

Figure S4. Liquid-liquid phase separation of aqueous of HEXD-V. (a) Timescale of changes in droplet size and refractive index, determined from fitting the Raman shift positions of the WGMs. (b) RH variation after the trapping chamber during the humidity changing process. (c) Time-resolved Raman spectra. The cessation of the random motion of inclusions within the droplet and the resultant formation of a core-shell structure are indicated by the grey dashed line on the left. The grey dashed line on the right serves as an indication of the point at which the droplet morphology transitions from a state of phase separation to a homogeneous phase morphology. This transformation is characterized by the occurrence of phase mixing.

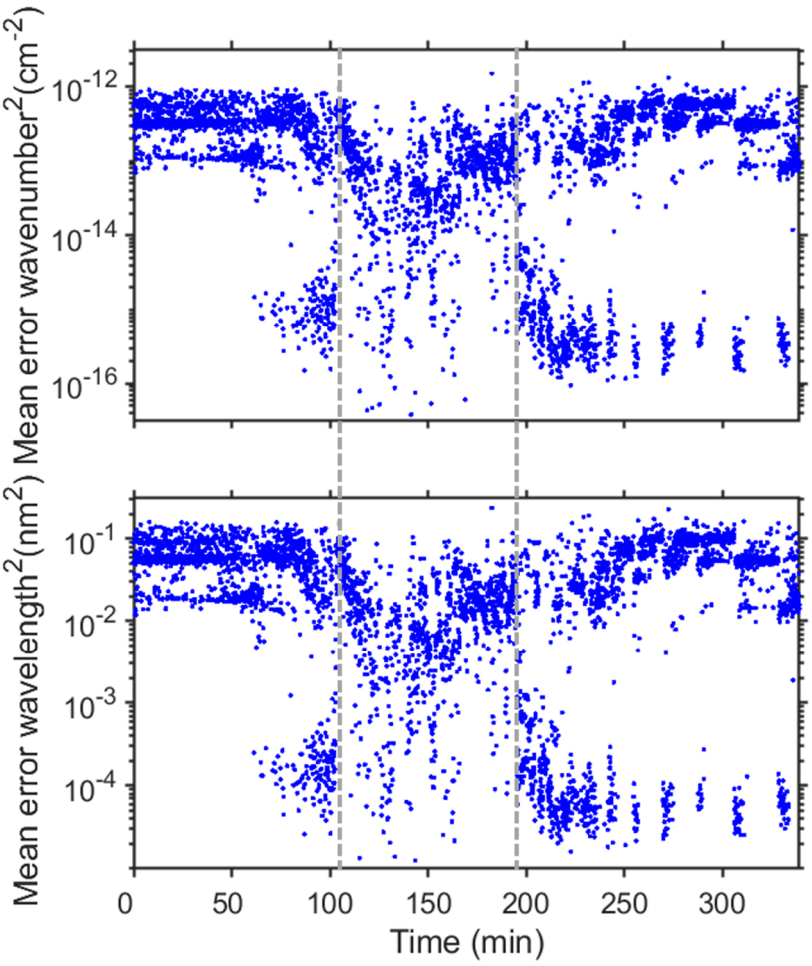

Figure S5. Fitting errors of the WGMs based on the homogenous Mie scattering model, corresponding to Figure 2 in the main text. The grey dashed lines indicated the moments of LLPS and phase mixing, respectively. The messy points in the figure primarily resulted from the errors generated during the batch peak finding process using the ipeak algorithm.

Table S1. Purity and suppliers of the compounds used in this study.

Compounds	Purity	Supplier
GL	99.5%	Meryer
3-MGA	99.0%	Macklin
HEXT	99.0%	TCI
HEXD	99.0%	Heowns Biochem LLC
AS	analytical reagent, >99%	Sinopharm chemical reagent
SA	analytical reagent, >99%	Sinopharm chemical reagent
NaOH	analytical reagent, 98.0%	Sinopharm chemical reagent

Table S2. Detailed SRH information of 3-MGA/AS system studied, as well as initial diameter, separation diameter (SD), separation relative index (SRI), MRH, mixing diameter (MD), and mixing relative index (MRI) data. Meanwhile, the last column presents the morphology of droplets when the llps occurred, core shell structure (CS) or partially-engulfed struture (PE).

Initial pH	Initial Dp (nm)	SRH (%)	SD (nm)	SRI (λ=650nm)	MRH (%)	MD (nm)	MRI (λ=650nm)	Morphology
0.48	9.86	69.5	6.02	1.576	83.5	6.82	1.540	CS
	12.08	69.8	8.45	1.454				PE
1.19	9.85	75.9	6.05	1.570	76.3	6.04	1.571	CS
	11.85	80.7	10.66	1.398	90.5	10.61	1.399	CS
	11.99	76.4	9.32	1.394	91.4	9.30	1.399	CS
2.7	8.99	75.6	6.62	1.559	84.5	6.71	1.566	CS
	12.21	82.6	9.03	1.401	90	9.01	1.400	CS
3.7	10.28	84.7	7.04	1.518				CS
	9.37	76.3	6.34	1.563				CS
	12.97	84.6	8.32	1.394				PE
5.21	12.92	89.2	9.02	1.364	89.5	7.89	1.381	CS
	10.37	89.8	8.74	1.374				CS
6.53	13.79	92.7	10.10	1.262	87.6	7.85	1.387	CS

Table S3. Detailed SRH information of HEXT/AS system studied, as well as initial diameter, separation diameter (SD), separation relative index (SRI), MRH, mixing diameter (MD), and mixing relative index (MRI) data. Meanwhile, the last column presents the morphology of droplets when the llps occurred.

Initial pH	Initial Dp (nm)	SRH (%)	SD (nm)	SRI (λ=650nm)	MRH (%)	MD (nm)	MRI (λ=650nm)	Morphology
0.92	14.04	75.7	10.58	1.438	85.7	10.83	1.420	CS
2.02	11.77	76.9	9.04	1.412				CS
	13.70	75.7	8.46	1.398				CS
	13.78	73.8	9.45	1.413				CS
	12.27	79.2	9.41	1.412	81.8	9.34	1.410	CS
3.14	11.14	77.3	8.44	1.407				CS
	13.10	78.1	9.38	1.410				CS
	12.39	74.7	9.05	1.408	81.3	9.04	1.409	CS
	12.60	76.2	9.18	1.408				CS
5.11	13.96	76.8	8.90	1.394	81.9	8.52	1.412	CS
	13.48	82.2	9.00	1.383				CS
	13.14	75.9	9.55	1.411	85.9	9.56	1.412	CS

Table S4. Detailed SRH information of HEXD/AS system studied, as well as initial diameter, separation diameter (SD), separation relative index (SRI), MRH, mixing diameter (MD), and mixing relative index (MRI) data. Meanwhile, the last column presents the morphology of droplets when the llps occurred.

Initial pH	Initial Dp (nm)	SRH (%)	SD (nm)	SRI (λ=650nm)	MRH (%)	MD (nm)	MRI (λ=650nm)	Morphology
1.39	11.28	82.4	8.64	1.375				CS
	12.35	68.0	7.96	1.414				CS
	10.82	69.9	7.83	1.408	81.2	7.93	1.406	CS
2.03	10.18	80.1	8.05	1.390				CS
	10.24	84.0	8.81	1.376				CS
	11.19	84.2	6.85	1.380	87.3	8.83	1.392	CS
2.71	13.20	78.8	8.24	1.391	89.1	8.44	1.389	CS
	14.54	78.9	8.61	1.382	91.8	8.89	1.377	CS
	15.91	75.3	8.06	1.400	88.0	8.27	1.397	CS
3.13	10.79	81.5	8.77	1.376				CS
	11.72	80.2	9.21	1.403	89.3	9.14	1.384	CS
	10.54	81.4	8.92	1.373				CS
5.01	10.20	81.4	8.77	1.362				CS
	10.55	75.5	8.01	1.393	89.7	8.00	1.393	CS
	15.09	81.2	8.20	1.397	89.5	8.76	1.387	CS